Multi-helical Lamb Wave Imaging for Pipe-like Structures Based on a Probabilistic Reconstruction Approach

Zhe Wang, Songling Huang, *Senior Member, IEEE,* Shen Wang,
Qing Wang, *Senior Member, IEEE,* and Wei Zhao

Abstract—**The special form of pipe-like structure provides the helical route for ultrasonic guided wave. Considering the pipe as a flattened plate but with periodical replications, the helical wave becomes intuitional and corresponding imaging algorithm can be constructed. This work proposes the multi-helical Lamb wave imaging method through utilizing the multiple arrival wavepackets which are denoted as different orders. The helical wave signal model is presented and the constant group velocity point is illustrated. The probabilistic reconstruction algorithm is combined with separation and fusion of different helical routes. To verify the proposed scheme, finite element simulations and corresponding experiments are conducted. The cases of single-defect simulation and two-defects simulation indicate the successful and robust implementation of the imaging algorithm. The test on actual pipe damage is also investigated to show its capability in imaging an irregular defect. The comparison with imaging results from only first arrival demonstrates the advantage of multi-helical wave imaging, including the better imaging resolution and higher localization accuracy.**

***Index Terms*—Defect imaging, helical wave, Lamb wave, pipe structure, probabilistic reconstruction.**

I. INTRODUCTION

THE visualization of damage is always the objective of structural health monitoring (SHM) [1]–[3]. The ultrasonic guided wave provides a potential scheme for the inspection and imaging of pipe-like structures for its long propagation distance and low attenuation [4]–[6]. Guided wave can interact with defects in its propagation path and through decoding the information contained in the received signal, the location and size of damage can be obtained [7], [8].

Guided wave of multiple modes can be generated in the pipe [9]. The axially propagating guided wave, including longitudinal and torsional modes, is commonly applied in current researches [10]–[12]. The electromagnetic acoustic transducer (EMAT) owns the non-contact characteristic and it can be used in a wide variety of applications [13]. Liu et al. designed the transducer with a multi-splitting meander coil to generate longitudinal mode with enhanced signal [14]. Nurmalia et al. applied a periodic permanent magnet to compose the EMAT and generated torsional waves for pipe inspection [15]. Recently, the helical wave attracted some researchers to utilize the spiral way to detect the damage in a particular extension direction [16]–[19]. However, current transducers are either omni-directional or unidirectional, which own certain disadvantages in generating helical wave in pipe structure. Research into helical Lamb wave, including the transducer design and corresponding post-processing techniques, is still in its infancy and needs further study. The transducer with a simple configuration was proposed to form the helical Lamb wave effectively and its performance was also investigated using the divergence angle [20]. The presented work is an extension of this preceding paper to further study the signal processing of helical wave.

After the guided wave generation and reception, the signal post-processing is vital for the localization and imaging of pipe defects [21]–[24]. Xu et al. introduced a ridge extraction technique in time-frequency domain to divide the signal into individual modes [25]. Huthwaite et al. developed the helical path separation outline to improve the viewing effect by utilizing multiple arrival wavepackets [26]. Kim et al. proposed the mode decomposition method based on the chirplet transform and it obtained individual modes from multimodal wavepackets [27]. Gao et al. combined broadband excitation and pulse compression to locate and assess the damage [28]. Hameed et al. applied continuous wavelet transformation and developed the multistage detection scheme to quantify the damage [29]. However, the overlapping phenomenon in helical Lamb wave presents in different forms and the corresponding processing and imaging method need to be investigated.

The appropriate post-processing provides the foundation for defect imaging [30]. Davies et al. implemented synthetic aperture focusing imaging on the pipe structure and measured its imaging responses at different defect positions [31]. However, it needs to control the multiple transducers to accomplish the focusing process, which increases the complexity. Leonard et al. proposed the helical ultrasound tomography algorithm based on the simultaneous iterative reconstructive technique [32]. Willey et al. regarded the damage imaging as an inverse problem and proposed the curved ray tomography technique to utilize the helical wave [33].

This research was financially supported by the National Key Research and Development Program of China (Grant No. 2018YFF01012802), National Natural Science Foundation of China (NSFC) (Grant No. 51677093 and No. 51777100)

Z. Wang, S. Huang, S. Wang, and W. Zhao are with the State Key Laboratory of Power System, Department of Electrical Engineering, Tsinghua University, Beijing 100084, China (e-mail: huangsling@mail.tsinghua.edu.cn).

Q. Wang is with the Department of Engineering, Durham University, Durham DH1 3LE, U.K.

Huthwaite et al. introduced the medical ultrasonic imaging method into guided wave tomography [34]. Livadiotis et al. presented an algebraic reconstruction imaging method for corrosion damage imaging based on the ray approximation [35]. These methods used the solutions for the classic inverse problem; however, usually the solutions are involved with iterative procedures and multiple parameters need to be set and adjusted according to different applications. Besides, the tomography based on the utilization of helical wave has not been fully investigated. The rapid and effective approach to dealing with multi-helical wave and achieve high-resolution imaging needs to be explored.

In this work, a multi-helical Lamb wave imaging approach is proposed based on the probabilistic reconstruction algorithm and the multi-helical route image fusion. The objective is to facilitate the analysis and usage of multi-helical wave to establish a highly detailed visualization of damage. Multiple transmitters and receivers are distributed along the pipe circumference to generate and receive the helical wave, respectively. The received wavepackets are firstly separated according to the group velocity. Then the signal information is applied to construct the signal difference coefficient (SDC) and realize the probabilistic reconstruction. Finally, the reconstruction results from different routes are combined and filtered to accomplish the imaging.

The remainder of this paper is organized as follows. Section II illustrates the helical Lamb wave EMAT and models the helical routes. In section III, the detailed description of the proposed method, which combines the multi-helical Lamb wave and probabilistic reconstruction algorithm, is provided. In section IV, the verification of the proposed method is conducted in finite element simulation firstly. Then the experimental investigation and corresponding comparisons are given in Section V. Concluding remarks are summarized in Section VI.

II. HELICAL LAMB WAVE EMAT AND HELICAL ROUTE

In previous study, the helical Lamb wave EMAT has been proposed and the generated wave could propagate along the structure in a spiral form [20], [36], [37]. The illustration of the EMAT and the helical routes are presented in Fig. 1. This EMAT is composed of permanent magnets and wire which is wrapped around the magnets. The wave superposition principle is used to design the geometrical parameters of the EMAT to enhance the signal and the Lorentz mechanism is utilized to generate the helical Lamb wave.

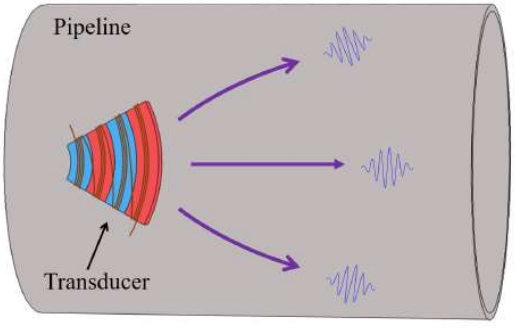

Fig.1. Illustration of the helical Lamb wave EMAT and the helical routes.

Due to the deliberately designed EMAT structure, the helical Lamb wave can propagate in multiple spiral angles and arrive at the defect after multiple turns. Thus, the wave can interact with the defect at different angles which can lead to more accurate defect imaging. To model and utilize the helical wave, the pipe-like structure is expanded to the flattened plate structure but with periodical repetitions. The unwrapped structure is illustrated in Fig. 2. The different replications of the plate structure are referred to as orders. The helical routes can be considered as the propagation in different orders. The physical transducers lie in the order 0. The transducers in the left and right sides of physical plate are virtual transducers. The orders are denoted as $\pm n_o$. The sign of "+" in Fig. 2 means that the helical wave propagates towards the right direction, while the sign of "-" means the left direction.

The received signal can be regarded as the summation of the signal from all the sensors corresponding to the same physical receiver and the signal model can be expressed as

$$\Theta(t) = \sum_{n_o} \theta_{r+Nn_o}(t). \tag{1}$$

where $\theta(t)$ is the separated time trace in different receivers, N is the number of the physical receiver, the subscript $r + N\ n_o$ indicates the notation of each receiver and $\Theta(t)$ is the aggregated received signal.

Lamb wave can be sorted into two types: symmetric (S) mode and anti-symmetric (A) mode. They can be expressed in following notation:

$$S \text{ mode}: \quad S_n,\ n = 0, 1, 2, \cdots \tag{2}$$

$$A \text{ mode}: \quad A_n,\ n = 0, 1, 2, \cdots. \tag{3}$$

The mathematical expression for Lamb wave can be described by the Rayleigh-Lamb equation [9]. Through solving this equation, the characteristic of dispersion can be obtained and is presented in Fig. 3. The dispersion means the velocity of wave varies with the product of frequency *(f)* and object thickness *(d)*. As the frequency or thickness changes, the wave velocity also varies to influence the wave propagation, which will bring difficulties in identifying the corresponding Lamb wave mode.

To overcome this drawback brought by dispersion, the constant group velocity (CGV) was proposed and exploited [38]. According to the theory of CGV, the group velocity of fundamental asymmetric mode A_0 remains constant in a wide region despite the thickness loss due to the corrosion. This CGV point is also represented in Fig. 3(a) using the diamond mark. It can be seen that in the region around this CGV, the dispersion curve of group velocity is nearly a horizontal line parallel to the abscissa axis. It means the group velocity is insensitive to the frequency and thickness. When guided wave is generated under the condition of the CGV point, the arrival time of guided wave packet is independent of the thickness and it will be unchanged, which makes the wavepackets easy to be recognized. The steady propagation of Lamb wavepackets will also improve the signal post-processing. However, the phase velocity is still sensitive to the variation of object thickness as shown in Fig. 3(b). Then the signal phase can contain the thickness loss information. The proposed approach will utilize this phase difference and image the defect.

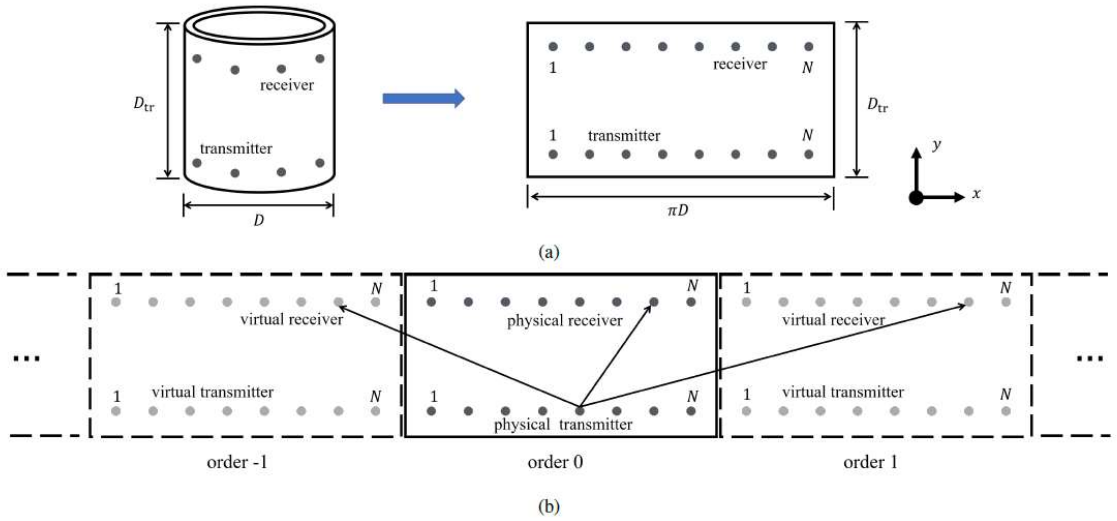

Fig. 2. The pipe-like structure is expanded to the flattened plate structure but with periodical repetitions. (a) The unwrapped structure. (b) The replications are referred to as different orders.

From Fig. 3(a), the CGV point appears in the frequency thickness product (f ·d) of around 1400 Hz · m. Thus, to utilize the CGV property, the helical Lamb needs to be generated under this condition. Since the thickness *(d)* of the pipe considered in this work is 6 mm, the excitation frequency *(f)* is set as 230 kHz to form the wave in CGV.

III. COMBINATION OF MULTI-HELICAL LAMB WAVE AND PROBABILISTIC RECONSTRUCTION ALGORITHM

To help understand the proposed method, the overall procedures are presented in Fig. 4. The detailed explanations are given below.

A. Probabilistic Reconstruction Algorithm

The imaging process is based on the correlation analysis of baseline signal and detection signal. This process is called a reconstruction algorithm for probabilistic inspection of damage (RAPID) [39]. The baseline signal can be obtained under normal conditions in which no damage occurs.

In detail, the SDC is measured between the baseline signal and detection signal. The mathematical expression is given below:

$$SDC = 1 - \rho \tag{4}$$

where ρ is the correlation coefficient and it can be expressed as:

$$\rho = \frac{C_{S_d S_b}}{\sigma_{S_d} \sigma_{S_b}} \tag{5}$$

where $C_{Sd\,Sb}$ is the covariance of detection signal S_d and baseline signal S_b. The covariance can be calculated by

$$C_{S_d S_b} = \sum_{i}^{T} (s_d(t_i) - \mu_d)(s_b(t_i) - \mu_b) \tag{6}$$

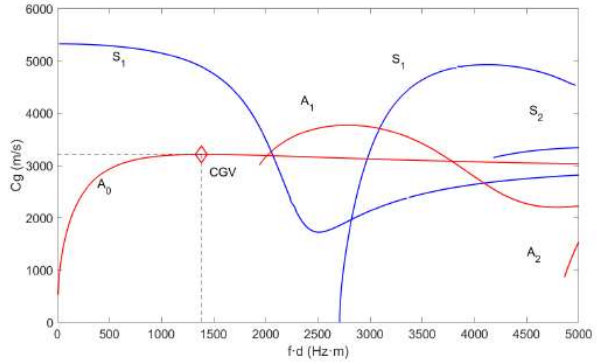

Fig. 3. The dispersion curve of Lamb wave. (a) The group velocity. (b) The phase velocity

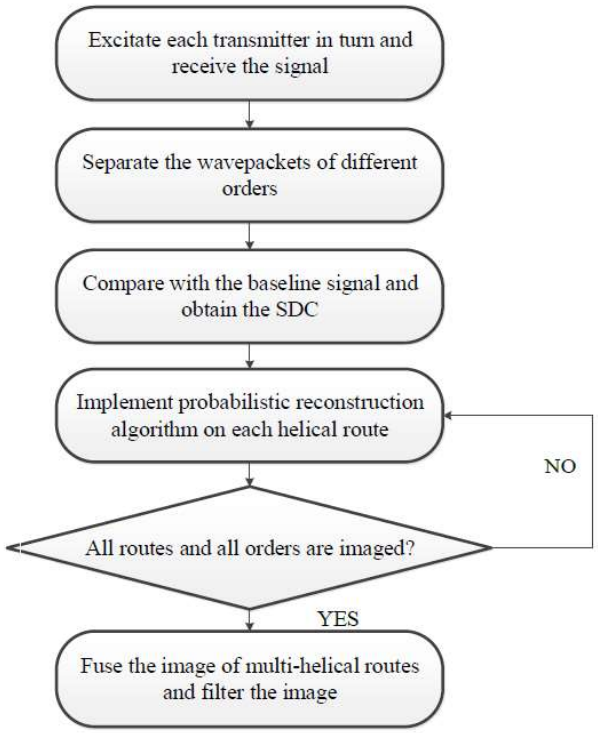

Fig. 4. The block diagram of the proposed method

where T is the length of the signal and μ is the mean of the respective signal. The $\sigma_{Sd}\,\sigma_{Sb}$ is the product of two standard deviations and it can be expressed as:

$$\sigma_{S_d}\sigma_{S_b} = \sqrt{\sum_{i}^{T}(s_d(t_i)-\mu_d)^2}\sqrt{\sum_{i}^{T}(s_b(t_i)-\mu_b)^2} \qquad (7)$$

The reconstructed image $P\,(x, y)$ is the summation of SDC from each transmitter-receiver pair:

$$P(x,y) = \sum_{k=1}^{N_p} p_k(x,y) = \sum_{k=1}^{N_p} SDC_k \times E_{ij}(x,y) \qquad (8)$$

where (x, y) is the grid in the coordinate system, N_p is the total number of the transmitter-receiver pair, $p_k\,(x, y)$ is the defect distribution estimation from each pair, and $E_{ij}\,(x, y)$ is the spatial distribution function. This distribution function owns the non-negative value and it can be expressed as:

$$E_{ij}(x,y) = \frac{\beta - R_{ij}(x,y)}{\beta - 1} \qquad (9)$$

where β is the parameter for scaling, and $R_{ij}\,(x, y)$ is the distance ratio between the indirect path and direct path linking the transmitter and receiver. The ratio is given in (10), in which (x_i, y_i) is the transmitter location and (x_j, y_j) is the receiver location. The largest $R_{ij}\,(x, y)$ is limited by the parameter β. The distribution function $E_{ij}\,(x, y)$ forms the elliptical region along the wave path and the results are shown in Fig. 5. The closer the distance between the imaging grid and the path, the higher the value of the distribution function.

B. Helical Routes Separation

The helical Lamb waves of different orders own different path lengths. Denote the axial distance between the transmitter and receiver as D_{tr}. Then the path length L of helical Lamb wave in transmitter-receiver pair can be expressed as:

$$L = \sqrt{D_{tr}^2 + (a + n_o \pi D)^2} \qquad (11)$$

where α is the initial circumferential distance of each transmitter-receiver pair and D is the pipe diameter. Due to the constant group velocity, the wavepacket of the same path length will appear in the same time in despite of the existence of defect. To separate the wavepackets of different orders, the rectangular window can be added to the entire signal to extract the individual wavepacket, since different orders own different propagation distances. The rectangular window is in time domain and its length can be chosen as the time duration slightly larger than that of the excitation signal. The excitation signal is usually a short pulse called tone-burst and the common expression is shown as:

$$P_u(t) = [0.54 - 0.46\cos(\frac{2\pi t}{T_u})] \cdot \sin(2\pi f_c t) \qquad (12)$$

where f_c is the center frequency, T_u is the total time duration. Then a larger value than T_u is proper for the time duration of the rectangular window.

According to the group velocity, the center time of rectangular window for every helical order can be given by:

$$c_o = \frac{L}{v_g} \qquad (13)$$

After obtaining individual wavepackets of each helical route, the separated signal can be compared with the baseline signal in turn. In the damage region, the thinning effect will lead to the change of phase velocity of helical Lamb wave. Thus, the variation of waveform will occur. The signal difference will be generated between the inspected signal and baseline signal. The probabilistic reconstruction algorithm can be applied to image the defect.

C. Image Fusion

The unwrapped version of pipe-like structure can be considered as a plate with replications. The helical route will pass through different regions of the flattened plate. Although the more orders of helical Lamb wave will bring the better defect image, it will cause the consumption of more CPU and memory sources. Besides, since the wave of the larger orders will propagate more times around the pipe, the signal strength becomes weaker and the interference will cover the useful information in the signal. Further, it needs more time and storage to pick up the signal. Therefore, in this work, only orders of 0, +1 and -1, namely the physical plate and two replications, are employed to accomplish the image fusion.

The reconstructed image $P\,(x, y)$ appears also in the plate replications and these regions can be projected to the plate of order 0. The image value in the same physical position will be summed to obtain the combined image:

$$R_{ij}(x,y)=\begin{cases}\dfrac{\sqrt{(x-x_i)^2+(y-y_i)^2}+\sqrt{(x-x_j)^2+(y-y_j)^2}}{\sqrt{(x_j-x_i)^2+(y_j-y_i)^2}}, & R_{ij}\le\beta\\ \beta, & R_{ij}>\beta\end{cases} \tag{10}$$

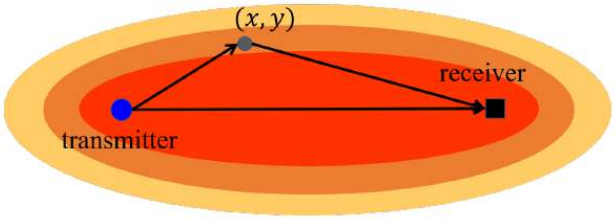

Fig.5. The elliptical distribution function in the probabilistic reconstruction algorithm.

$$I(x,y)=\sum_{n_o}P(x,y) \tag{14}$$

Finally, the image is filtered by the common median filter [40]. In the imaging results, the larger image values will indicate the location and relative severity of defect. In the following sections, the simulations and experiments will be conducted to verify the proposed method.

IV. SIMULATION VERIFICATION

The verification of the proposed method is firstly carried out in the finite element simulation. Eight transmitters and eight receivers are distributed evenly around the pipe circumference. The axial distance of the transmitter and receiver is set as 300 mm. The Youngs modulus, density and Poissons ratio are set as 205 GPa, 7850 kg · m^{-3} and 0.28, respectively. The post-processing of the signal is implemented using the computational software MATLAB.

A. One Defect Case

The one regular defect is constructed on the pipe, which is just in front of transmitter #3 with a distance of 200 mm. Its diameter is set as 80 mm. The corresponding flattened plate and replicated version are shown in Fig. 6. The acoustic ray routes from the transmitter #3 are depicted. The defect also appears in the replicated regions. It can be seen that due to the multiple helical Lamb wave, the wave can pass through the defect at different angles.

The eight transmitters are excited in turn and all receivers will receive the signal in each transmission. It means that every receiver will pick up eight waveform data and in total 64 waveform data will be obtained. The data will be sorted and stored in the computer for further analysis. In Fig. 7, it presents the waveform from eight receivers when the third transmitter #3 is excited. It clearly shows that the helical Lamb waves from different orders arrive at the receivers at different times. In the same helical route order, the wavepackets reach to the different receivers in sequence. In each waveform, multiple wavepackets appear which means the wave propagates in a helical way and waves of multiple orders can be detected. The wavepackets of order -2 appear in the waveforms of part of the receivers because some of the routes own short distances.

The baseline signal is obtained in the same way but no defect is constructed on the pipe. To illustrate the variation brought by the defect, the waveform of receiver #5 and the corresponding baseline signal are shown in Fig. 8. It can be seen that the wavepackets arrive at the same time under the faultless and defect situations. However, the wavepackets are not overlapped totally in time domain. For receiver #5, the helical route of order 1 passes through the defect while order 0 and -1 do not. In the waveforms, larger variations can be observed in the third wavepackets of order 1. Therefore, the signal presents different phase information due to the defect.

The imaging approach is employed on the received signal. The scaling parameter β is set as 1.05. The results from three orders of helical routes are shown in Fig. 9. In each order, some imaging values indicating potential defects could be found. Besides order 0, the routes in order -1 and 1 also propagate through the defect and the signal difference contributes to the imaging values.

After the image fusion and simple median filtering, the results are presented in Fig. 10. To compare the obtained image with the true defect, the shape of the actual defect is also depicted and it is in red circle. It clearly shows that the fused image keeps consistent with the true defect. The location of the obtained image coincides with that of the circle defect. However, the result of defect region is slightly larger than the actual defect area. This is because the SDC has an effect on the entire propagation route and brings the expansion of the defect imaging region.

B. Case with Two Defects

In this case, two defects are constructed on the pipe. One is just in front of transmitter # 3 same with the one defect case, while another one is in front of transmitter #6 with a central distance of 100 mm. The illustration can be seen in Fig. 11(a). The two defects have different sizes and their diameters are 80 and 40 mm, respectively.

The imaging results are shown in Fig. 11(b). It can be observed that the imaging value in the bigger defect is larger than that in the smaller defect. It can be inferred that the correlativity exists between the image value and defect severity degree. Further analysis indicates that this relation presents the tendency of correlation, but it is not strictly linear and the mathematical model is difficult to be calculated. Therefore, the imaging results also contain the information about the defect size or defect depth, which can be applied to make alert for the pipe maintenance. It can also be noticed that the region between the two defects owns certain imaging values. Although this region brings interference to the defect recognition, it does not

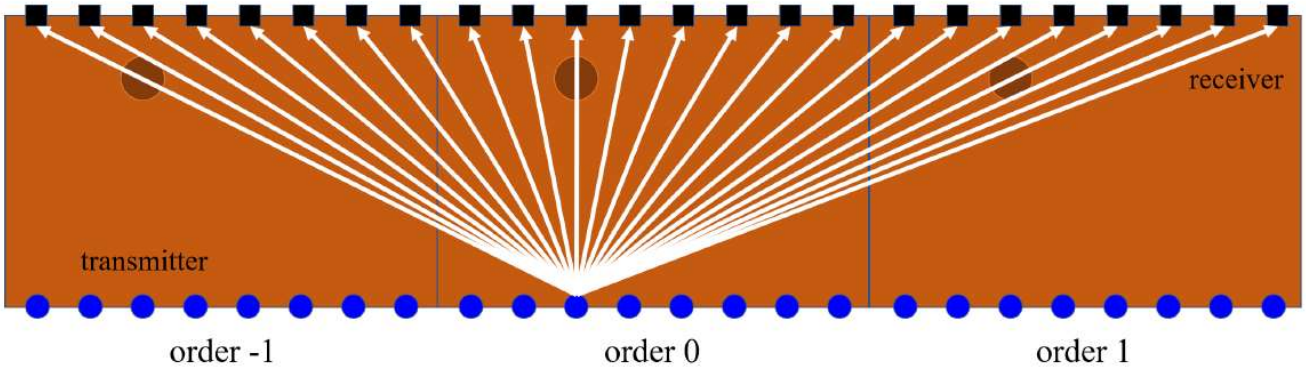

Fig.6. The flattened plate and replicated virtual plate. The one regular defect is constructed as the circle. The acoustic ray routes from the transmitter #3 are depicted. The helical wave propagates through the defect in different angles.

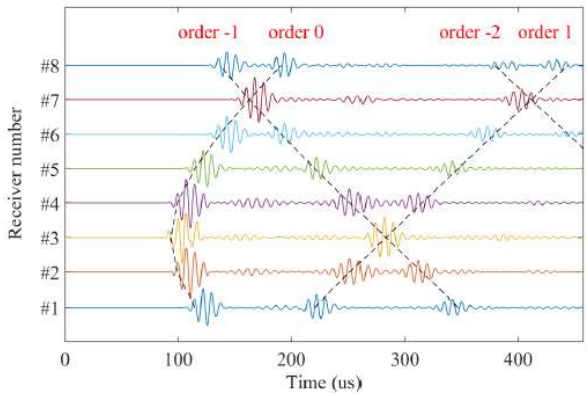

Fig.7. The waveform from eight receivers when the transmitter #3 is excited.

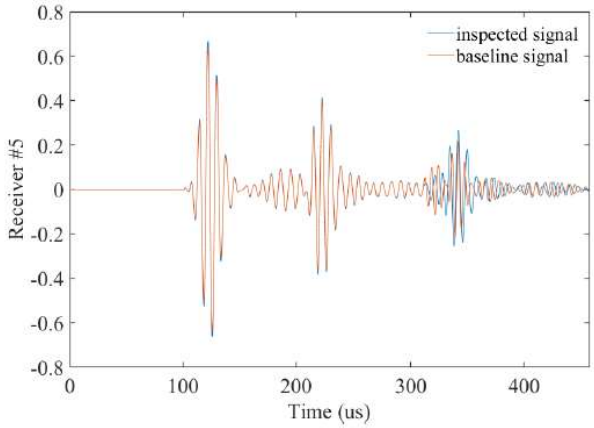

Fig.8. The waveforms from receiver #5 and the corresponding baseline signal.

influence the distinguishing of these two different defects. Similarly, the imaging region is larger than the actual size. This is the shortcoming of the probabilistic reconstruction algorithm. The threshold method or advanced filtering scheme needs to be developed to optimize the imaging results.

V. EXPERIMENTAL INVESTIGATION

The corresponding experimental system is established on the pipe. The transducers and receivers are set up the same as those in the simulations. The block diagram of experimental system is shown in Fig. 12(a). The RITEC RPR-4000 (Ritec Inc., Warwick, RI) is adopted as the pulser and receiver for helical Lamb wave. The impedance matching networks composed of basic circuit components are used to optimize the wave signal.

A. Random Damage Brought by Corrosion

One site of metal loss exists in the pipe and it is the damage to be inspected and imaged. The photograph of this damage is shown in Fig. 12(b). This defect presents an irregular form due to the corrosion factor in its environment. The axial direction of pipe is also depicted in the figure. To image the pipe, the baseline signal is firstly obtained from one section of pipe in its pristine state where no damage occurs. Then the detection signal is measured from the inspected pipe section. The waveforms from transducer pair of #5 - #5 are shown in Fig. 12(c). It can be observed that the defect influences the direct wavepacket and causes the signal difference because the direct route passes through the defect. The other two orders (-1 and 1) of wavepackets are overlapped since they own the same propagation distance. The waveforms of these two orders are consistent between the inspected signal and baseline signal because the helical routes propagate in areas without defect. Compared with the pure wavepacket in simulations, the noise with small amplitude appears though the signal is filtered. After the implementation of the proposed algorithm, the imaging results can be obtained and are shown in Fig. 13(a). It can be seen that the main imaging values appear in the position of the corrosion defect. Some interferences also appear in the upper left and upper right sides. The formation of these small imaging values is caused by the rough surface in corresponding pipe positions, which influences the inspected signal and causes the signal difference. The tendency and profile in the imaging results conform to the actual damage. Therefore, this algorithm presents good performance in imaging the irregular defect.

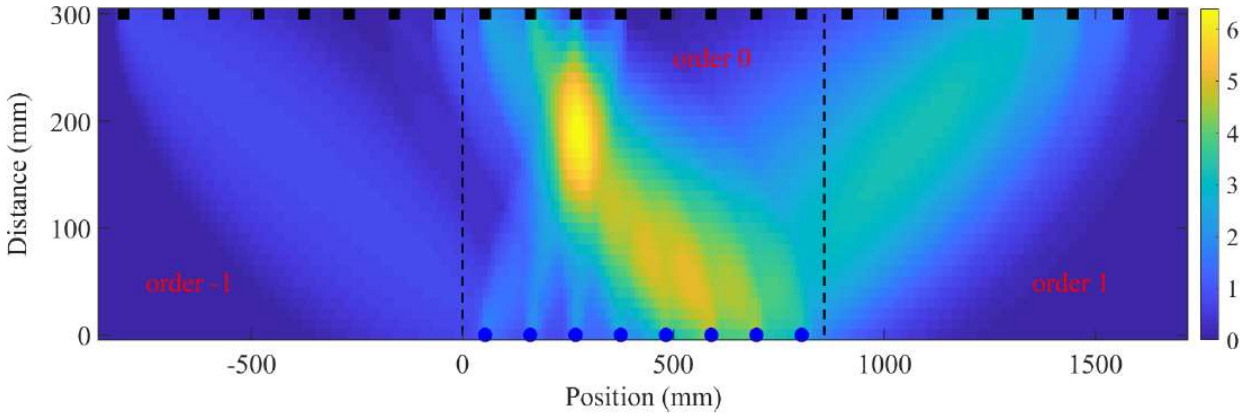

Fig.9. The imaging results of utilizing three orders helical Lamb wave. The three orders are presented separated by the dark dotted lines

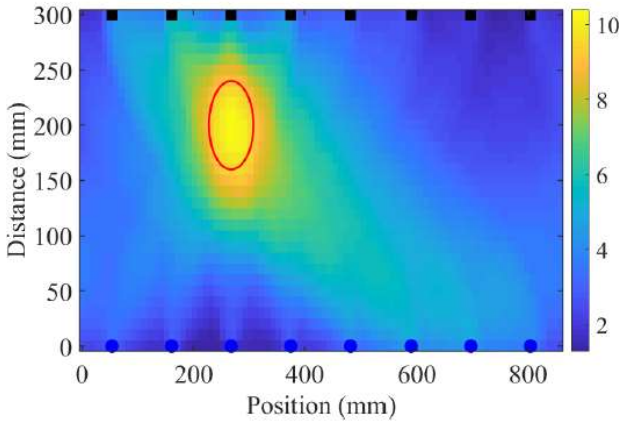

Fig.10. The imaging result after the fusion of three orders and simple median filtering.

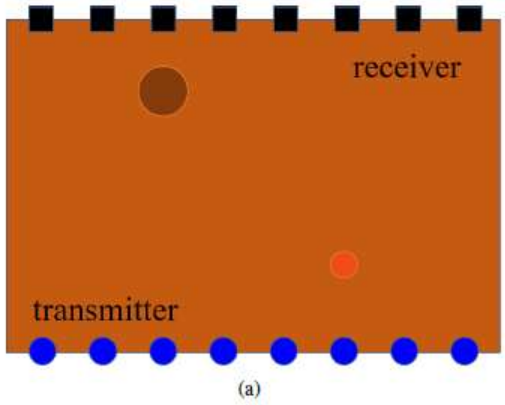

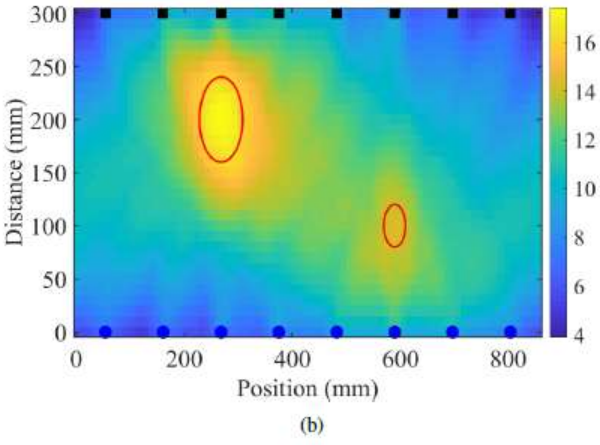

Fig. 11. The case of two defects in the finite element analysis. (a) The illustration of the defect sizes and positions. (b) The imaging results for the case of two defects.

B. Comparison and Analysis

Usually in the traditional imaging scheme of plate or pipelike structure, only the first arrival wavepacket of signal is extracted for further analysis. Due to the ring structure of pipe, multiple helical routes could reach to the receivers and three orders are considered in aforementioned section. For comparison, only the first arrival wavepacket is utilized to image the defect. The results are shown in Fig. 13(b). The imaging values present the location of the defect; however, the indicated shape is different from the actual form. The overall imaging values are not detailed enough. The edge between background and the defect region shows abrupt characteristics and more interferences exist in the whole imaging region. This is because of the lack of imaging information compared with the multi-helical imaging results.

Further, the imaging values along the axial distance of 100 mm in Fig. 13(a) and (b) are normalized to indicate the depth values. The biggest value and the smallest value are adjusted to 0 and 1, respectively. The depth of the actual defect is also measured. The deepest part and the pipe surface are denoted as 0 and 1, respectively. Then the results are depicted in Fig. 14. To quantify the accuracies of these two schemes, the localization of defect is conducted and the results are given in Table I. The deepest values of the multi-helical wave imaging and the first arrival wavepacket imaging appear at 464 mm and 505 mm, respectively. The true deepest part appears at 454 mm. Then the relative errors can be calculated and they are 2.2% and 11.2%, respectively. It can be observed that the multi-helical

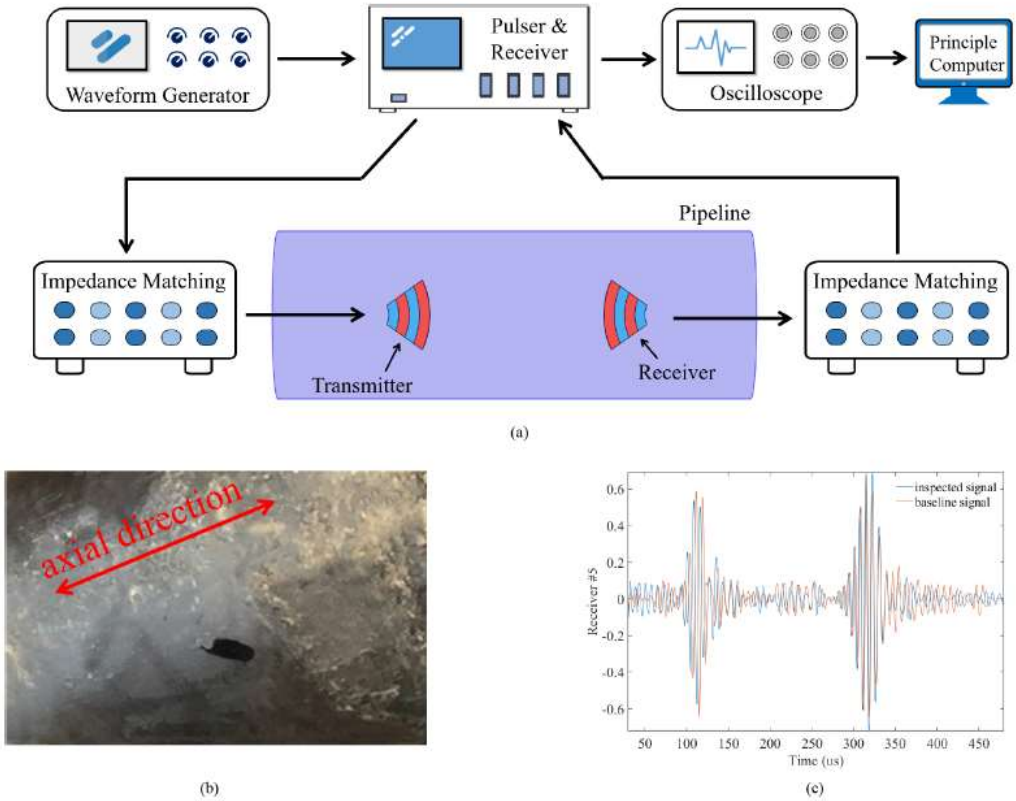

Fig.12. The experiment carried on the random damage in actual pipe. (a) The diagram of experimental system. (b) The damage photograph. (c) The detection signal and baseline signal for the transducer pair (# 5 - # 5).

TABLE I
LOCALIZATION ERROR COMPARISON OF THE DEEPEST PART IN DEFECT

Method	Calculated Location	True Location	Relative Error
Multi-helical Wave Imaging	464 mm	454 mm	2.2%
Direct Wave Imaging	505 mm	454 mm	11.2%

scheme presents higher accuracy in the localization of the defect, while the imaging by the first arrival shows a certain of position mismatch compared with the true location. Therefore, the multi-helical utilization is superior to the traditional first-arrival imaging.

Theoretically, this reconstruction method is based on the straight ray assumption of acoustic wave. This assumption is suitable for cases of high frequency, for example, X-rays. However, the frequency of helical Lamb wave is not high and a certain of error might be generated. In some situations, the phenomenon of bent ray might occur and the acoustic route will be changed. Thus, the imaging resolution will be degraded. Compared with tomography based on solutions of wave fields, the resolution of this work is lower. However, the wave field method needs complex calculations and large memory for data storage. In all, the proposed method can obtain the imaging with simple computation and relative high resolution.

VI. CONCLUSIONS

In this work, an imaging method is proposed to utilize the multi-helical Lamb wave, which propagates along the pipe structure in a spiral form. The pipe can be extended into a flattened plate structure but with periodical replications. The physical plate and two replications, or a total of three orders, are considered to provide the high-resolution imaging. The one-defect simulation in finite element analysis indicates that the proposed algorithm can localize and describe the defect region. The two-defects simulation shows that although blur imaging values exist in the middle parts between these two defects, the recognition of this two defects is still available. The experimental investigations and corresponding comparison are also conducted. The imaging scheme using multiple arrival wavepackets presents better imaging resolution. In addition, after the conversion to depth value, the multi-helical scheme also owns higher localization accuracy. Therefore, the proposed method could be a potential and practical tool in actual defect imaging. In future research, the damage quantization capability requires further study to facilitate the utilization of helical wave.

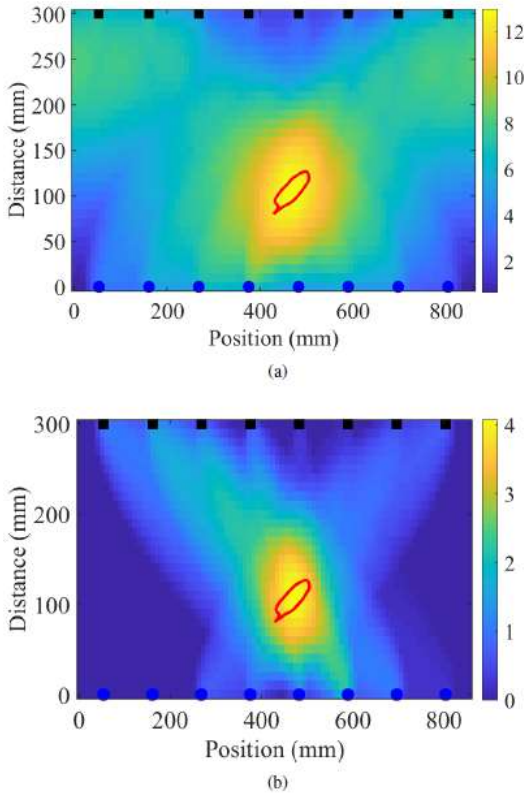

Fig.13. The imaging results for the pipe damage. (a) The result of imaging method using multi-helical wave. (b) Only the first arrival wavepacket is utilized to image the defect.

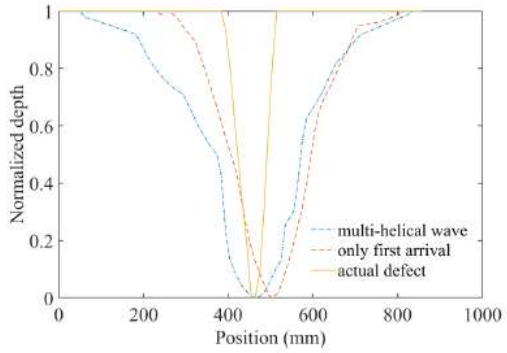

Fig. 14. The imaging values along the axial distance of 100 mm are converted to the depth values

REFERENCES

[1] A. Bagheri, P. Rizzo, and K. Li, "Ultrasonic imaging algorithm for the health monitoring of pipes," Journal of Civil Structural Health Monitoring, vol. 7, no. 1, pp. 99–121, 2017.

[2] A. Golato, F. Ahmad, S. Santhanam, and M. G. Amin, "Multi-helical path exploitation in sparsity-based guided-wave imaging of defects in pipes," Journal of Nondestructive Evaluation, vol. 37, no. 2, p. 27, 2018.

[3] J. Laviada, B. Wu, M. T. Ghasr, and R. Zoughi, "Nondestructive evaluation of microwave-penetrable pipes by synthetic aperture imaging enhanced by full-wave field propagation model," IEEE Transactions on Instrumentation and Measurement, vol. 68, no. 4, pp. 1112–1119, 2019.

[4] N. Nakamura, H. Ogi, and M. Hirao, "EMAT pipe inspection technique using higher mode torsional guided wave T (0, 2)," NDT & E International, vol. 87, pp. 78–84, 2017.

[5] U. Amjad, S. K. Yadav, and T. Kundu, "Detection and quantification of pipe damage from change in time of flight and phase," Ultrasonics, vol. 62, pp. 223–236, 2015.

[6] Z. Wang, S. Huang, S. Wang, S. Zhuang, Q. Wang, and W. Zhao, "Compressed sensing method for health monitoring of pipelines based on guided wave inspection," IEEE Transactions on Instrumentation and Measurement, vol. 69, no. 7, pp. 4722–4731, 2020.

[7] X. Chen, X. Li, S. Wang, Z. Yang, B. Chen, and Z. He, "Composite damage detection based on redundant second-generation wavelet transform and fractal dimension tomography algorithm of lamb wave," IEEE Transactions on Instrumentation and Measurement, vol. 62, no. 5, pp. 1354–1363, 2013.

[8] B. Feng, D. J. Pasadas, A. L. Ribeiro, and H. G. Ramos, "Locating defects in anisotropic cfrp plates using tof-based probability matrix and neural networks," IEEE Transactions on Instrumentation and Measurement, vol. 68, no. 5, pp. 1252–1260, 2019.

[9] J. L. Rose, Ultrasonic guided waves in solid media. Cambridge university press, 2014.

[10] H. W. Kim, Y. E. Kwon, J. K. Lee, and Y. Y. Kim, "Higher torsional mode suppression in a pipe for enhancing the first torsional mode by using magnetostrictive patch transducers," IEEE transactions on ultrasonics, ferroelectrics, and frequency control, vol. 60, no. 3, pp. 562–572, 2013.

[11] R. Guan, Y. Lu, W. Duan, and X. Wang, "Guided waves for damage identification in pipeline structures: A review," Structural Control and Health Monitoring, vol. 24, no. 11, pp. e2007–n/a, 2017.

[12] J. He, C. Zhou, L. Yang, and X. Sun, "Research on pipeline damage imaging technology based on ultrasonic guided waves," Shock and Vibration, vol. 2019, pp. 1–18, 2019.

[13] N. Lunn, S. Dixon, and M. D. G. Potter, "High temperature emat design for scanning or fixed point operation on magnetite coated steel," NDT and E International, vol. 89, pp. 74–80, 2017.

[14] Z. Liu, Y. Hu, J. Fan, W. Yin, X. Liu, C. He, and B. Wu, "Longitudinal mode magnetostrictive patch transducer array employing a multisplitting meander coil for pipe inspection," NDT & E International, vol. 79, pp. 30–37, 2016.

[15] Nurmalia, N. Nakamura, H. Ogi, and M. Hirao, "Mode conversion and total reflection of torsional waves for pipe inspection," Japanese Journal of Applied Physics, vol. 52, no. 7, 2013.

[16] H. W. Kim, H. J. Lee, and Y. Y. Kim, "Health monitoring of axiallycracked pipes by using helically propagating shear-horizontal waves," NDT & E International, vol. 46, pp. 115–121, 2012.

[17] H. W. Kim, J. K. Lee, and Y. Y. Kim, "Circumferential phased array of shear-horizontal wave magnetostrictive

patch transducers for pipe inspection," Ultrasonics, vol. 53, no. 2, pp. 423–431, 2013.

[18] B. Hu, N. Hu, L. Li, W. Li, S. Tang, Y. Li, X. Peng, A. Homma, Y. Liu, L. Wu, and H. Ning, "Tomographic reconstruction of damage images in hollow cylinders using lamb waves," Ultrasonics, vol. 54, no. 7, pp. 2015–2023, 2014.

[19] F. Simonetti and M. Y. Alqaradawi, "Guided ultrasonic wave tomography of a pipe bend exposed to environmental conditions: A long-term monitoring experiment," NDT & E International, vol. 105, pp. 1–10, 2019.

[20] Z. Wang, S. Huang, S. Wang, Q. Wang, and W. Zhao, "EMAT design for defect inspection in pipe-like structure using helical lamb wave," in 2020 IEEE International Instrumentation and Measurement Technology Conference (I2MTC), 2020, pp. 1–5.

[21] S. Legendre, D. Massicotte, J. Goyette, and T. K. Bose, "Wavelettransform-based method of analysis for Lamb-wave ultrasonic NDE signals," IEEE Transactions on Instrumentation and Measurement, vol. 49, no. 3, pp. 524–530, 2000.

[22] A. Velichko and P. D. Wilcox, "Post-processing of guided wave array data for high resolution pipe inspection," J Acoust Soc Am, vol. 126, no. 6, pp. 2973–82, 2009.

[23] H. Z. Hosseinabadi, B. Nazari, R. Amirfattahi, H. R. Mirdamadi, and A. R. Sadri, "Wavelet network approach for structural damage identification using guided ultrasonic waves," IEEE Transactions on Instrumentation and Measurement, vol. 63, no. 7, pp. 1680–1692, 2014.

[24] P. Wang, W. Zhou, and H. Li, "A singular value decomposition-based guided wave array signal processing approach for weak signals with low signal-to-noise ratios," Mechanical Systems and Signal Processing, vol. 141, p. 106450, 2020.

[25] K. Xu, D. Ta, and W. Wang, "Multiridge-based analysis for separating individual modes from multimodal guided wave signals in long bones," IEEE transactions on ultrasonics, ferroelectrics, and frequency control, vol. 57, no. 11, pp. 2480–2490, 2010.

[26] P. Huthwaite and M. Seher, "Robust helical path separation for thickness mapping of pipes by guided wave tomography," IEEE Transactions on Ultrasonics, Ferroelectrics, and Frequency Control, vol. 62, no. 5, pp. 927–938, 2015.

[27] C.-Y. Kim and K.-J. Park, "Mode separation and characterization of torsional guided wave signals reflected from defects using chirplet transform," NDT & E International, vol. 74, no. Supplement C, pp. 15–23, 2015.

[28] F. Gao, L. Zeng, J. Lin, and Y. Shao, "Damage assessment in composite laminates via broadband lamb wave," Ultrasonics, vol. 86, pp. 49–58, 2018.

[29] M. S. Hameed, Z. Li, J. Chen, and J. Qi, "Lamb-wave-based multistage damage detection method using an active PZT sensor network for large structures," Sensors (Basel, Switzerland), vol. 19, no. 9, p. 2010, 2019.

[30] A. B. Zoubi, S. Kim, D. O. Adams, and V. J. Mathews, "Lamb wave mode decomposition based on Cross-Wigner-Ville distribution and its application to anomaly imaging for structural health monitoring," IEEE Transactions on Ultrasonics, Ferroelectrics, and Frequency Control, vol. 66, no. 5, pp. 984–997, 2019.

[31] J. Davies and P. Cawley, "The application of synthetic focusing for imaging crack-like defects in pipelines using guided waves," IEEE Transactions on Ultrasonics, Ferroelectrics, and Frequency Control, vol. 56; 56, no. 4; 4, pp. 759–771, 2009.

[32] K. R. Leonard and M. K. Hinders, "Lamb wave tomography of pipe-like structures," Ultrasonics, vol. 43, no. 7, pp. 574–583, 2005.

[33] C. L. Willey, F. Simonetti, P. B. Nagy, and G. Instanes, "Guided wave tomography of pipes with high-order helical modes," NDT & E International, vol. 65, pp. 8–21, 2014.

[34]] P. Huthwaite and F. Simonetti, "High-resolution guided wave tomography," Wave Motion, vol. 50, no. 5, pp. 979 – 993, 2013.

[35] S. Livadiotis, A. Ebrahimkhanlou, and S. Salamone, "An algebraic reconstruction imaging approach for corrosion damage monitoring of pipelines," Smart Materials and Structures, vol. 28, no. 5, p. 55036, 2019.

[36] Z. Wang, S. Huang, S. Wang, Q. Wang, and W. Zhao, "Design of electromagnetic acoustic transducer for helical lamb wave with concentrated beam," IEEE Sensors Journal, vol. 20, no. 12, pp. 6305–6313, 2020.

[37] Z. Wang, S. Wang, Q. Wang, W. Zhao, and S. Huang, "Development of a helical lamb wave electromagnetic acoustic transducer for pipeline inspection," IEEE Sensors Journal, vol. 20, no. 17, pp. 9715–9723, 2020.

[38] P. B. Nagy, F. Simonetti, and G. Instanes, "Corrosion and erosion monitoring in plates and pipes using constant group velocity lamb wave inspection," Ultrasonics, vol. 54, no. 7, pp. 1832–1841, 2014.

[39] T. R. Hay, R. L. Royer, H. Gao, X. Zhao, and J. L. Rose, "A comparison of embedded sensor Lamb wave ultrasonic tomography approaches for material loss detection," Smart Materials and Structures, vol. 15, no. 4, pp. 946–951, 2006.

[40] L. Tan and J. Jiang, "Chapter 13 - image processing basics," in Digital Signal Processing (Third Edition). Academic Press, 2019, pp. 649 – 726.